

Tube shape selection for heat recovery from particle-laden exhaust gas streams

T G Walmsley, M R W Walmsley*, M Atkins, J Neale & J Hoffman-Vocke

*contact e-mail: m.walmsley@waikato.ac.nz

Abstract

Heat recovery from exhaust gas streams is applicable to a wide variety of industries. Two problems encountered in exhaust gas heat recovery are: the high heat transfer resistance of gases and the presence of entrained particulate matter, which can limit the use of extended surface area. Standard heat exchangers use round tube. This study uses Computational Fluid Dynamics (CFD) to investigate whether round or another shape is the best tube selection for exhaust heat recovery.

Tube shape rankings are based on taking into account heat transfer, gas flow resistance and foulability. Foulability is inferred from the average wall shear stress around the front or back of each shape. An estimated asymptotic fouling resistance is used to calculate an equivalent fouled j factor, j_f . CFD results suggest the best tube for exhaust heat recovery is an elliptical tube. The ellipse shape produced j/f and j_f/f ratios (where f is the tube bank friction factor) over 1.5 times larger than that of standard round tube. A flattened round tube is also promising and may be the practical and economic optimum.

Introduction

Many industrial processes produce hot exhaust gas streams. These processes can vary significantly in terms of scale and application. Three New Zealand examples are gas fired turbines in electricity generation, coal fired boilers for process heating, and spray dryers in dairy and food powder production. In each case the process draws in fresh cool gas and emits hot humid gas, which carries with it a substantial quantity of waste heat. A simple method to increase overall process efficiency is to recover the heat from the exhaust gas stream and use it to pre-heat the cool incoming gas stream or another heat sink.

Two significant problems are encountered in exhaust gas heat recovery: the high heat transfer resistance of gases and the presence of entrained particulate matter. In boiler recuperators, a particulate foulant layer 2 mm thick can reduce the overall heat transfer coefficient by 5% [1]. Foulant layers also increase heat exchanger pressure drop and may prove difficult to remove. For many cases, the use of extended area surfaces is not recommended [1]. In particular, fins are prone to deformation during cleaning resulting in an overall long-term performance drop.

Traditionally, compact heat exchangers use standard round tube. Round tube is widely available and offers a favourable heat transfer to pressure drop ratio. Geometrically, it has no localised stress concentrations, meaning wall thickness can be kept to a minimum. However recent studies suggest other shaped tubes show better performance than round tube, especially when subjected to fouling [2–4].

A key selection in heat exchanger design is the tube shape. This study numerically investigates the trade-off between heat transfer, pressure drop, and foulability of 10 tube shapes. Particular attention is given to fouling in two locations, the front and back of the tube. Sub-micron particles are controlled by a diffusion transport mechanism and deposit at the rear of tubes, whereas larger

particles are inertia impaction controlled and deposit on the front of tubes. The addition of extended area surfaces, such as fins, and in-line tube arrangement are not considered.

Theory

Heat transfer and pressure drop

The heat transfer coefficient, h , of a heat exchanger surface is calculated using the Colburn j factor,

$$h = \frac{c_p \rho}{Pr^{2/3}} \frac{u_\infty}{\sigma} j \quad (1)$$

Where c_p is the gas heat capacity, ρ is the gas density, Pr is the Prandtl number, u_∞ is average gas face velocity, and σ is the frontal free-flow area. The power per heat transfer area, E , needed to overcome a tube banks core friction (ignoring flow acceleration effects, which typically accounts for about 1 – 3% of the pressure drop) is,

$$E \cong \Delta P \frac{u_\infty}{\sigma} = \frac{1}{2} \rho \left(\frac{u_\infty}{\sigma} \right)^3 f \quad (2)$$

Where ΔP is the tube bank pressure drop. In this study the Reynolds number, Re , is defined as $Re = \rho \varphi / \mu \cdot u_\infty / \sigma$, where μ is the gas viscosity and φ is the hydraulic gas diameter. Efficient heat exchanger surfaces have a favourable h/E ratio,

$$h/E \cong \frac{2c_p}{Pr^{2/3} u_\infty^2} \sigma^2 j / f \quad (3)$$

Eq. 3 shows j/f is proportional to h/E for a given face velocity. Higher j/f ratios will result in more heat transfer for the same amount of fan power, which indicates a more efficient heat exchanger surface. To make a fair comparison, σ and α (and, therefore, φ) are held constant for the different tube shapes.

Heat exchanger fouling

Shah & Sekulic [6] review several particulate deposition and re-entrainment models. Assuming particulate fouling is asymptotic [7], then the general time dependent model has the form,

$$R_f = \frac{A}{\tau_w} \left(1 - e^{-\frac{\tau_w t}{B}} \right) \quad (4)$$

Where R_f is the fouling resistance, τ_w is the wall shear stress, t is time, constants A and B are proportional to a combination of gas velocity, particulate concentration, and transport coefficients. Taking the limits as time becomes large,

$$R_f(t \rightarrow \infty) = \frac{A}{\tau_w} \quad (5)$$

We may define equivalent fouled heat transfer coefficient, h_f , and fouled j factor, j_f , are,

$$h_f = \left[\frac{1}{h} + R_f \right]^{-1} = \left[\frac{1}{\left(\frac{c_p \rho}{Pr^{2/3}} \frac{u_\infty}{\sigma} \right) j} + \frac{A}{\tau_w} \right]^{-1} \rightarrow j_f = \left[\frac{1}{j} + \frac{\left(\frac{c_p \rho}{Pr^{2/3}} \frac{u_\infty}{\sigma} \right) A}{\tau_w} \right]^{-1} \quad (6)$$

Very thick foulant layers may result in a R_f about 0.0005 m²·°C/W, which roughly corresponds to $A = 0.0005$ Pa·m²·°C/W. This A value is used to translate average τ_w into approximate R_f values.

Methods

Tube geometries and Numerical models

Tube geometries (Figure 1a) include: (1) round, (2) 90° diamond (or rotated square), (3) 75° diamond, (4) hexagon, (5) ellipse (2:1), (6) egg (front-side 2:1 ellipse, back circle), (7) reverse egg, (8) 90° apex round (9) reverse 90° apex round and (10) flattened round (20 mm flats). The hydraulic gas diameter, φ , is constant for all geometries. This is achieved by using a constant $\sigma = 0.33$ and $\alpha = 83 \text{ m}^2/\text{m}^3$. Initial values were taken from the standard arrangement of 20 mm diameter round tube with a transverse spacing ratio of 1.5 (30 mm) and longitudinal spacing ratio of 1.25 (25 mm). To hold α constant, the longitudinal spacing is varied.

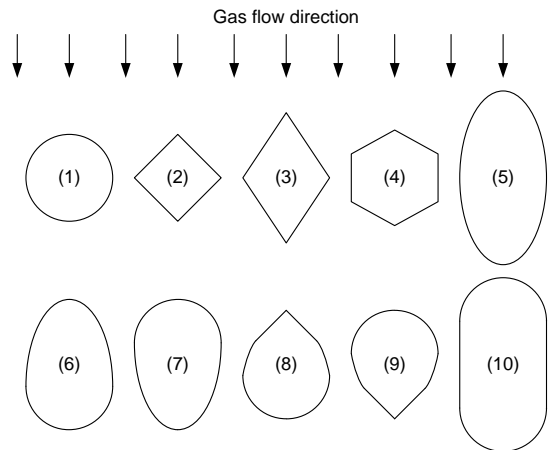


Figure 1: Tube geometries and orientation to gas flow direction.

Two-dimensional Computational Fluid Dynamics (CFD) models in Fluent 13.0 have been developed. Each model contains six rows of tube (Figure 2). The mesh was verified to be solution independent. Wall boundary layers were inflated to obtain a wall $y^+ < 1$. As a result the cell numbers were in the order of 10^5 for all geometries. The inlet and outlet lengths and inlet gas turbulence were also tested for solution independence. Three turbulence models were used to solve the round tube model: the $k-\Omega$ Shear Stress Transport (SST), Realizable $k-\Omega$ and Reynolds-Normalisation Group (RNG) $k-\Omega$ models. The SST turbulence model produced the closest match to experimental correlations [5,8,9] (Figure 3) and was also used in all other tube models.

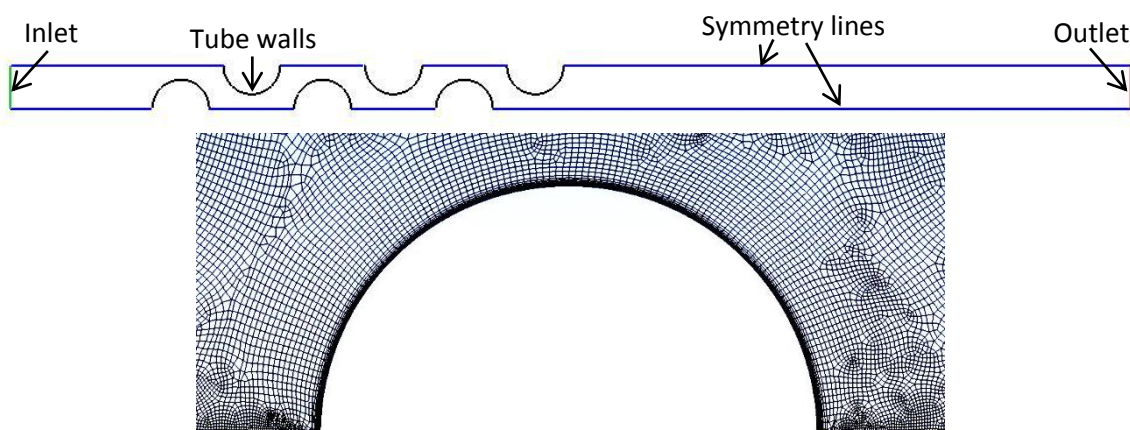


Figure 2: Round tube model and mesh.

The inlet temperature was set at 350 K and the wall temperature at 300 K. To reduce the flow entrance development effects, heat transfer was only modelled on the 4th and 5th rows. Heat transfer on the front rows are significantly influenced by the developing gas flow. Temperature and pressure drop outputs are converted into dimensionless numbers j and f . Area averaged wall shear

stress values are calculated for the front and back facing sides. Sides parallel to the flow are not included in the averages. Figure 3 shows the CFD derived data accurately represents the experimental correlations. The most significant difference occurred at low Re ; the friction factor deviation was 9%, which is still within the experimental error [5].

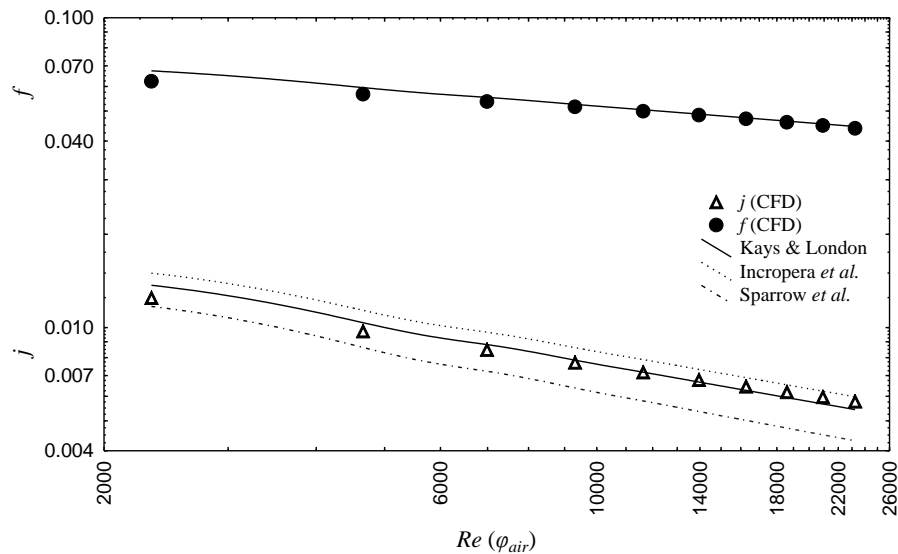


Figure 3: Comparison of j and f values from literature experimental correlations to CFD predictions for round tube [5,8,9].

Results and discussion

Tube performance results are summarised and ranked (**Error! Reference source not found.**). Each factor is divided by the round tube equivalent. For example, the 90° diamond obtained the highest j factor. On average across the Re range of 2,300 – 24,000, j for the 90° diamond was 41% higher than round tube, or a ratio of 1.41.

Table 1: Summary of tube geometry performance ratios.

Ranking	$(Nu)^*$	$(f)^*$	$\left(\frac{Nu}{f}\right)^*$	$(\tau_w)^*$ (Front)	$(Nu_f)^*$ (Front)	$\left(\frac{Nu_f}{f}\right)^*$ (Front)	$(\tau_w)^*$ (Back)	$(Nu_f)^*$ (Back)	$\left(\frac{Nu_f}{f}\right)^*$ (Back)
Ellipse	0.74	0.35	2.29	0.65	0.75	2.17	1.04	1.09	3.16
Flattened round	0.82	0.47	1.80	0.93	0.88	1.85	1.33	1.14	2.40
Reverse egg	0.88	0.68	1.37	0.91	0.97	1.42	1.00	1.07	1.58
Egg	0.95	0.74	1.27	0.84	0.87	1.17	1.12	1.08	1.45
Apex	0.98	0.91	1.07	0.95	0.95	1.05	0.94	0.94	1.03
Reverse apex	0.98	0.95	1.03	1.00	0.99	1.04	1.08	1.06	1.12
Round	1.00	1.00	1.00	1.00	1.00	1.00	1.00	1.00	1.00
75° Diamond	1.22	2.22	0.52	1.43	1.24	0.56	1.63	1.45	0.65
Hexagon	1.31	3.11	0.40	1.96	1.51	0.49	1.80	1.62	0.52
90° Diamond	1.46	3.55	0.39	1.89	1.54	0.43	2.33	2.00	0.56

* All values have been divided by the performance of round tube and average across all Re modelled.

The ellipse shape is predicted to give the best j/f and j/f ratios. An interesting observation is an ellipse has a lower j factor than round, but this is offset by a much lower f . In fact, all the shapes ranked above the round show a similar trend, whereas the shapes ranked below round have a slightly larger j , but over double the f . The second ranked tube shape is the flattened round tube. It

is expected that production costs of a flattened round tube is cheaper than elliptical tube. Flattened round tube is manufactured by rolling round tube to flatten the sides, whereas elliptical tube is non-standard in stainless steel in New Zealand. Hence, the flattened round tube may represent the economic optimum.

The tubes with pointed fronts had the highest τ_w , which infers they have the lowest foulability. In the cases of the 75° diamond, 90° diamond and hexagon shapes the benefit of low foulability was offset by the high f . The pointed fronts on these tubes contributed to the high f by creating a natural flow separation point and large recirculation zone (Figure 4a). This also means the maximum velocity in the 90° diamond (27.5 ms^{-1}) was 57% higher than for round. The low pressure drop of the ellipse is the result of a small rear recirculation zone.

Two limitations of this study are the cost of production and required tube wall thickness are not considered. The tube cost is linked to the amount of processing required (welds and shaping) and material used, which is also related to tube wall thickness. Future work will look at the cost, wall thickness and validation of the best performing shapes through experimental tests.

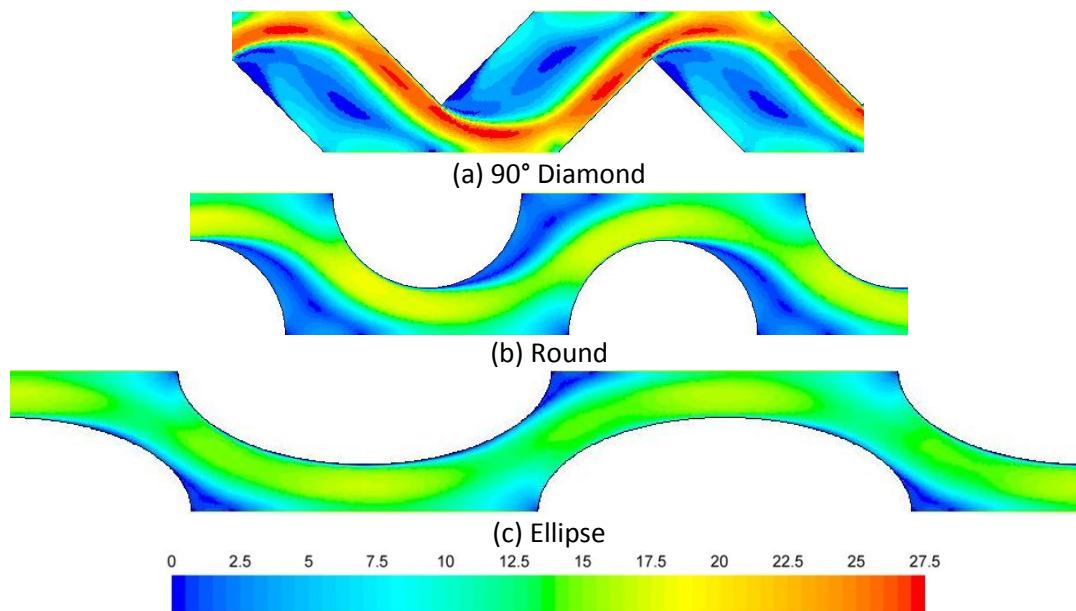


Figure 4: Magnitude velocity (ms^{-1}) contours around rows 4 and 5 at $u_\infty = 5 \text{ ms}^{-1}$ and $Re = 11,600$ (CFD).

Conclusion

Taking into account heat transfer, gas flow resistance and foulability, the recommended tube for exhaust gas heat recovery is elliptical tube. The ellipse shape produced a j/f ratio 2.1 times higher than standard round tube. The j_j/f based on the front and back wall shear stress was 1.54 and 1.59 times higher than round tube, respectively. The flattened round tube is also promising and may be the practical economic solution.

References

- [1] P. Stehlík, Applied Thermal Engineering 31 (2011) 1-13.
- [2] M.S. Abd-Elhady, C.C.M. Rindt, A.A. Van Steenhoven, Heat Transfer Engineering 32 (2011) 272 - 281.
- [3] D. Bouris, E. Konstantinidis, S. Balabani, D. Castiglia, G. Bergeles, International Journal of Heat and Mass Transfer 48 (2005) 3817-3832.
- [4] G. Zhang, T.R. Bott, C.R. Bemrose, Heat Transfer Engineering 13 (1992) 81-87.
- [5] W.M. Kays, A.L. London, Compact Heat Exchangers, 3rd ed., Krieger Pub. Co., 1998.
- [6] K.R. Shah, D.P. Sekulić, Fundamentals of Heat Exchanger Design, Wiley & Sons, Hoboken, NJ, 2003.
- [7] R. Webb, N. Kim, Principles of Enhanced Heat Transfer, 2nd ed., Taylor & Francis, Boca Raton, 2005.

- [8] E.M. Sparrow, J.P. Abraham, J.C. Tong, *International Journal of Heat and Mass Transfer* 47 (2004) 5285–5296.
- [9] F.P. Incropera, D.P. DeWitt, (2002).